

# Distributional Vision Language Alignment by Cauchy-Schwarz Divergence

Wenzhe Yin<sup>1\*</sup>, Zehao Xiao<sup>1\*</sup>, Pan Zhou<sup>3†</sup>, Shujian Yu<sup>4,5</sup>,  
Jiayi Shen<sup>1</sup>, Jan-Jakob Sonke<sup>2</sup>, Efstratios Gavves<sup>1</sup>

<sup>1</sup>University of Amsterdam, <sup>2</sup>The Netherlands Cancer Institute, <sup>3</sup>Singapore Management University

<sup>4</sup>Vrije Universiteit Amsterdam, <sup>5</sup>The Arctic University of Norway

## Abstract

Multimodal alignment is crucial for various downstream tasks such as cross-modal generation and retrieval. Previous multimodal approaches like CLIP utilize InfoNCE to maximize mutual information, primarily aligning pairwise samples across modalities while overlooking distributional differences. In addition, InfoNCE has inherent conflict in terms of alignment and uniformity in multimodality, leading to suboptimal alignment with modality gaps. To overcome the limitations, we propose CS-Aligner, a novel framework that performs distributional vision-language alignment by integrating Cauchy-Schwarz (CS) divergence with mutual information. CS-Aligner captures both the global distribution information of each modality and the pairwise semantic relationships. We find that the CS divergence seamlessly addresses the InfoNCE’s alignment-uniformity conflict and serves complementary roles with InfoNCE, yielding tighter and more precise alignment. Moreover, by introducing distributional alignment, CS-Aligner enables incorporating additional information from unpaired data and token-level representations, enhancing flexible and fine-grained alignment in practice. Experiments on text-to-image generation and cross-modality retrieval tasks demonstrate the effectiveness of our method on vision-language alignment.

## 1 Introduction

Modality alignment aims to map the paired modal inputs (e.g., text and image) into a shared feature space, enabling success across diverse applications such as image-text retrieval [1, 2], text-to-image (T2I) generation [3, 4], and multimodal chatbots [5]. As a pioneering work in this field, CLIP [6] leverages InfoNCE loss (a.k.a. contrastive loss) to maximize the mutual information between paired text and image representations, effectively capturing pairwise and semantic relationships. Its versatility has made it a foundation for many multimodal tasks [3, 7].

Despite its success, CLIP and its variants [8, 9] exhibit a persistent modality gap, a misalignment between text and image representations in the shared latent space. As shown in Fig. 1a, text and image embeddings often fail to align precisely and may remain separated from each other. This phenomenon has been widely observed [10–12] and is attributed to issues such as cone effects [11] or suboptimal latent space geometry [12]. Intriguingly, Liang *et al.* [11] observed that CLIP’s InfoNCE loss could inadvertently exacerbate the modality gap, since, as analyzed in Sec. 2, InfoNCE loss can be decomposed into alignment and uniformity components, which indeed conflict with each other during multimodal alignment.

\*Equal contribution

†Correspondence to: Pan Zhou <panzhou@smu.edu.sg>.

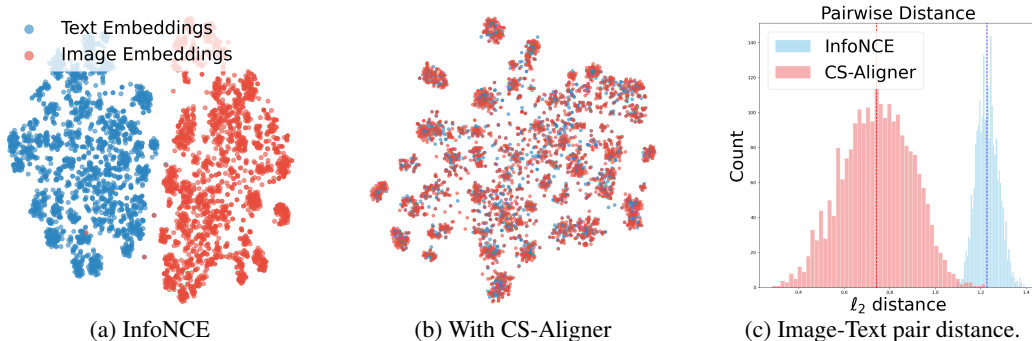


Figure 1: **TSNE visualizations of CLIP text and image features without (a) and with (b) CS-Aligner.** The original CLIP feature distributions reveal a clear domain gap (a). Adapting the model with our CS-Aligner effectively eliminates the modality gap, leading to tighter alignment (b). Consequently, CS-Aligner yields a lower overall  $\ell_2$  distance between paired image-text features (c).

Several strategies have been proposed to mitigate the modality gap, such as projection modules with cosine similarity [1, 10, 13] and geodesic multimodal mixup [14]. UnCLIP-based models like DALL-E 2 [3] and Kandinsky [4] employ text-to-image prior modules (e.g., diffusion models) to map text embeddings to image feature space for alignment. A more recent alternative Eclipse [15] uses  $\ell_2$  loss to train a prior adapter for text and image alignment. These works aim to transform representations across modalities for alignment. However, they explore alignment sample-wisely, heavily relying on pairwise data. Although sample-wise alignment effectively captures semantic information, it falls short in aligning entire data distributions. Similar to the InfoNCE in CLIP, the methods struggle to match the representation spaces across modalities, ultimately limiting the overall alignment. The reliance on carefully curated text-image pairs also limits the scalability and applicability to real-world scenarios with unpaired and noisy datasets [16, 17]. Moreover, the theoretical conflict of InfoNCE for multimodal alignment is still under exploration.

To address these challenges, we propose CS-Aligner, a novel distributional approach that incorporates Cauchy-Schwarz (CS) divergence [18] for modality alignment. As a symmetric measure, CS divergence robustly and efficiently estimates the distance between any representation distributions without parametric distributional assumptions, making it highly suitable for multimodal distribution alignment. Furthermore, we analyze the inherent conflict between alignment and uniformity in InfoNCE within the multimodal setting, and find that CS divergence can effectively mitigate the conflict and remains compatible with InfoNCE by estimating via a kernel density estimator (KDE) [19]. This enables CS-Aligner to align vision and language representations in both distributional and sample-wise levels, considering both the global modality and local semantic information, leading to more comprehensive, consistent, and tighter alignment as shown in Fig. 1b and Fig. 1c.

Moreover, the distributional nature of CS-Aligner enables alignment with unpaired multimodal data, including cases where a) a single image is associated with multiple captions, or b) vision and language inputs are entirely unpaired. This flexibility allows our method to leverage rich and unstructured datasets and improve alignment robustness beyond curated benchmarks. Beyond unpaired alignment, we introduce a token-level alignment strategy, which further enriches the multimodal representation by aligning fine-grained visual and textual tokens, enhancing the semantic precision of the learned embeddings. Extensive experiments on downstream tasks, including T2I generation and image-text retrieval, demonstrate the effectiveness of our approach.

## 2 InfoNCE is insufficient for alignment

Previous multimodal methods like CLIP [6] learn text and image representations in a shared space by maximizing lower bounds (e.g., InfoNCE [20]) of mutual information between modalities:

$$I(\mathbf{x}; \mathbf{y}) = \int \int p(\mathbf{x}, \mathbf{y}) \log \frac{p(\mathbf{x}, \mathbf{y})}{p(\mathbf{x})p(\mathbf{y})} d\mathbf{x} d\mathbf{y}, \quad (1)$$

where  $p(\mathbf{x})$  and  $p(\mathbf{y})$  are respectively the distributions of image and text features, and  $p(\mathbf{x}, \mathbf{y})$  denotes their joint probability. Although widely used, it suffers from two limitations.

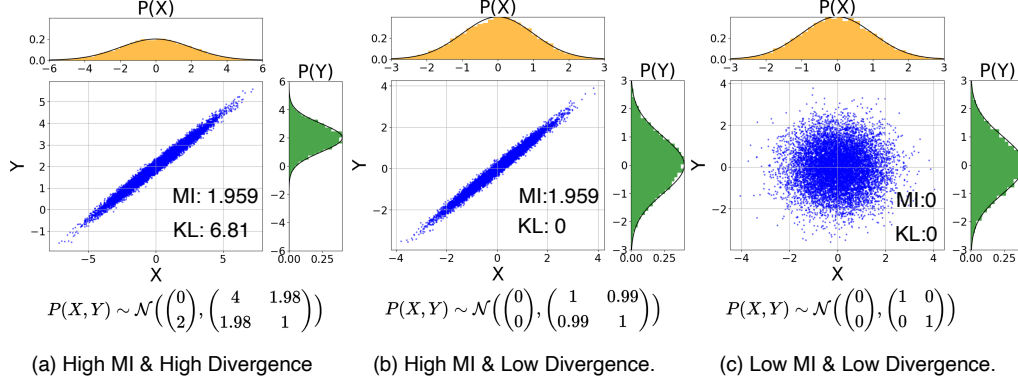


**Figure 2: Toy examples: mutual information (MI  $\uparrow$ ) and distributional divergence ( $\downarrow$ ) between two distributions.** Distributions with the same high mutual information value can exhibit either large (a) or small (b) distributional distances, demonstrating that MI alone is insufficient for multimodal alignment. Moreover, distribution divergence measures the closeness between distributions but does not guarantee that the underlying random variables are statistically correlated (c).

**Limitation1: Mutual information is insufficient for multimodal alignment.** Although widely adopted, mutual information alone is insufficient for effective modality alignment [11]. The reason is that mutual information quantifies the statistical dependence between two random variables [21], ensuring correlation maximization between two random variables. However, it does not guarantee that the distributions  $p(\mathbf{x})$  and  $p(\mathbf{y})$  are statistically similar or close to each other in terms of their underlying distributions. In other words, the embedding distributions of two modalities can differ significantly or be far apart, yet exhibit strong dependence.

We illustrate this issue using a toy example in Fig. 2. Fig. 2a shows that despite strong dependence and high mutual information, the representation distributions of two representations or random variables can remain misaligned and be far from each other, resulting in a high divergence. This issue is also observed in the CLIP model pretrained with InfoNCE, where the vision and language representations exhibit a noticeable distributional gap, as shown in Fig. 1a. This gap results in inconsistently aligned multimodal features, hindering the clear representation of shared semantics and disrupting effective mapping between modalities. Ultimately, this misalignment degrades performance in downstream tasks, including cross-modality generation. Ideally, the desired multimodal representations should be highly correlated with low distributional divergence, as depicted in Fig. 2b. Notably, although directly minimizing the divergence between distributions may reduce the distributional gap, it risks creating independent multimodal distributions without common semantic information (Fig. 2c). Therefore, maximizing mutual information and minimizing divergence complement each other to achieve effective multimodal representation alignment. Details are provided in Appendix B.

**Limitation2: InfoNCE includes conflicting terms for multimodal alignment.** In practice, mutual information is often optimized via minimizing the InfoNCE loss [20] which estimates  $I(\mathbf{x}; \mathbf{y})$  using paired image-text data  $\{(\mathbf{x}_i, \mathbf{y}_i)\}_{i=1}^N$  and contains image-text and text-image alignment terms:

$$\mathcal{L}_{\text{InfoNCE}} = -\frac{1}{2N} \sum_{i=1}^N (h(\mathbf{x}_i, \mathbf{y}_i) + h(\mathbf{y}_i, \mathbf{x}_i)), \quad h(\mathbf{x}, \mathbf{y}) = \log \frac{\exp(\text{sim}(\mathbf{x}, \mathbf{y})/\tau)}{\sum_{j=1}^N \exp(\text{sim}(\mathbf{x}, \mathbf{y}_j)/\tau)}, \quad (2)$$

where  $\text{sim}(\cdot, \cdot)$  is cosine similarity and  $\tau$  is temperature. Critically, the InfoNCE loss in Eq. (2) requires paired data  $\{(\mathbf{x}_i, \mathbf{y}_i)\}_{i=1}^N$ , and cannot work under unpaired setting.

As analyzed in [22], the InfoNCE loss can be decomposed as the sum of the alignment and uniformity terms i.e.,  $\mathcal{L}_{\text{InfoNCE}} \approx \mathcal{L}_{\text{align}} + \mathcal{L}_{\text{uniform}}$ :

$$\begin{aligned} \text{Alignment:} \quad \mathcal{L}_{\text{align}} &\triangleq \mathbb{E}_{(\mathbf{x}, \mathbf{y}) \sim p_{\text{pair}}} [\|\mathbf{x} - \mathbf{y}\|_2^\alpha], \\ \text{Uniformity:} \quad \mathcal{L}_{\text{uniform}} &\triangleq \log \mathbb{E}_{\mathbf{x}, \mathbf{y} \sim p(\mathbf{x}, \mathbf{y})} [\exp(-t\|\mathbf{x} - \mathbf{y}\|_2^2)], \end{aligned} \quad (3)$$

where  $t$  and  $\alpha$  are hyperparameters.  $p_{\text{pair}}$  denotes the image-text pairs distribution. Minimizing  $\mathcal{L}_{\text{align}}$  encourages pairwise alignment. In unimodality, minimizing  $\mathcal{L}_{\text{uniform}}$  promotes representations that are uniformly distributed on the unit hypersphere, a desirable property for representation learning [22]. However, in multimodal alignment,  $\mathcal{L}_{\text{uniform}}$  may conflict with  $\mathcal{L}_{\text{align}}$ .

**Remark 2.1.** The uniformity and alignment terms in InfoNCE conflict with each other in multimodal alignment. Applying Taylor expansions ( $\mathbb{E}(e^{-\mathbf{x}}) \approx 1 - \mathbb{E}(\mathbf{x})$  and  $\log(1 - \mathbf{x}) \approx -\mathbf{x}$ ) on  $\mathcal{L}_{\text{uniform}}$ , the uniformity term becomes:

$$\mathcal{L}_{\text{uniform}} \approx -t\mathbb{E}_{\mathbf{x}, \mathbf{y} \sim p(\mathbf{x}, \mathbf{y})} [\|\mathbf{x} - \mathbf{y}\|_2^2] = -t\mathbb{E}_{(\mathbf{x}, \mathbf{y}) \sim p_{\text{pair}} + p_{\text{unpair}}} [\|\mathbf{x} - \mathbf{y}\|_2^2], \quad (4)$$

where  $p(\mathbf{x}, \mathbf{y}) = p_{\text{pair}} + p_{\text{unpair}}$ , and  $p_{\text{unpair}}$  denotes the distribution of unpaired image and text. Consequently, the combination of the two (InfoNCE) can be written as:

$$\mathcal{L}_{\text{align}} + \mathcal{L}_{\text{uniform}} \approx \mathbb{E}_{(x, y) \sim p_{\text{pair}}} [\|\mathbf{x} - \mathbf{y}\|_2^\alpha] - t\mathbb{E}_{(\mathbf{x}, \mathbf{y}) \sim p_{\text{pair}} + p_{\text{unpair}}} [\|\mathbf{x} - \mathbf{y}\|_2^2]. \quad (5)$$

The alignment contribution ( $\mathcal{L}_{\text{align}}$ ) in Eq. (3) can be largely suppressed or even canceled (when  $t = 1$ ) due to the opposing term in Eq. (5), leaving only negative pairs influential. Essentially,  $\mathcal{L}_{\text{align}}$  promotes alignment across modalities, whereas  $\mathcal{L}_{\text{uniform}}$  encourages dissimilarity among negative pairs *without preserving intra-modal structure*. This inherent conflict can result in local minima, driving alignment and uniformity in opposing directions and ultimately leading to a modality gap. Thus, InfoNCE alone may lead to suboptimal alignment between modalities.

### 3 Methodology

In this section, we address the incapability of mutual information on aligning distributions and the conflicts in InfoNCE for multimodal alignment. To this end, we first introduce a novel distributional multimodal alignment framework, CS-Aligner. Then, we analyze that with the KDE, the proposed method is able to address the uniformity-alignment conflicts of InfoNCE. Finally, we extend CS-Aligner to the unpaired data, including token-level alignment.

#### 3.1 CS-Aligner: distributional multimodal alignment

To mitigate limitation 1 in Sec. 2, we explicitly minimize the distribution divergence between  $p(\mathbf{x})$  and  $p(\mathbf{y})$ . In practice,  $p(\mathbf{x})$  and  $p(\mathbf{y})$  may follow arbitrary distributions with minimal intersection, which may often occur in the multimodal setting. Hence, a robust divergence metric must accommodate unpredictable variability and limited support overlap for effective distribution alignment.

To this end, we propose a distributional alignment framework, namely **CS-Aligner**, which leverages the Cauchy-Schwarz divergence ( $D_{\text{CS}}$ ) [18, 23], as illustrated in Fig. 3. The objective is:

$$\min -I(\mathbf{x}; \mathbf{y}) + \lambda D_{\text{CS}}(p(\mathbf{x}), p(\mathbf{y})), \quad (6)$$

where  $\lambda$  is a hyperparameter balancing the mutual information term and the divergence penalty. CS divergence,  $D_{\text{CS}}$ , is a symmetric and robust metric to quantify the distance between any two probability density functions  $p$  and  $q$ , defined over the same support  $\omega$  as:

$$D_{\text{CS}}(p; q) = -\log \left( \left( \int p(\omega)q(\omega)d\omega \right)^2 / \left( \int p(\omega)^2 d\omega \int q(\omega)^2 d\omega \right) \right), \quad (7)$$

The CS divergence satisfies  $0 \leq D_{\text{CS}} < \infty$ , and equals zero if and only if  $p = q$ . By introducing  $D_{\text{CS}}$  in Eq. (6), instead of solely minimizing pairwise distance, our method also aligns the distributions of modalities, leading to more robust and efficient multimodal alignment, as shown in Fig. 3.

**CS divergence estimation.** To estimate CS divergence, we introduce non-parametrical KDE [19], eliminating the need for explicit parametric assumptions about the underlying distributions. This provides significant flexibility in measuring distributional distance. Given *i.i.d.* samples  $\{\mathbf{x}_i\}_{i=1}^M \sim p(\mathbf{x})$  and  $\{\mathbf{y}_i\}_{i=1}^N \sim p(\mathbf{y})$ , the empirical CS divergence estimator is given by [24]:

$$\hat{D}_{\text{CS}}(p(\mathbf{x}); p(\mathbf{y})) = \log \left( \frac{1}{M^2} \sum_{i,j=1}^M \kappa(\mathbf{x}_i, \mathbf{x}_j) \right) + \log \left( \frac{1}{N^2} \sum_{i,j=1}^N \kappa(\mathbf{y}_i, \mathbf{y}_j) \right) - 2 \log \left( \frac{1}{MN} \sum_{i=1}^M \sum_{j=1}^N \kappa(\mathbf{x}_i, \mathbf{y}_j) \right). \quad (8)$$

where  $\kappa$  is a kernel function such as Gaussian  $\kappa_\sigma(\mathbf{x}, \mathbf{y}) = \exp(-\|\mathbf{x} - \mathbf{y}\|_2^2 / 2\sigma^2)$  with kernel width  $\sigma$ . This estimator is symmetric, differentiable, and computationally efficient, making it suitable for multimodal alignment. Moreover, the third term in Eq. (8) ensures that  $\hat{D}_{\text{CS}}(p(\mathbf{x}); p(\mathbf{y})) \rightarrow \infty$  only when  $\mathbb{E}(\kappa(\mathbf{x}, \mathbf{y})) \rightarrow 0$  (i.e., when the distributions do not overlap). However, as long as there is a nonzero overlap between the distributions, the estimator remains well-defined and valid.



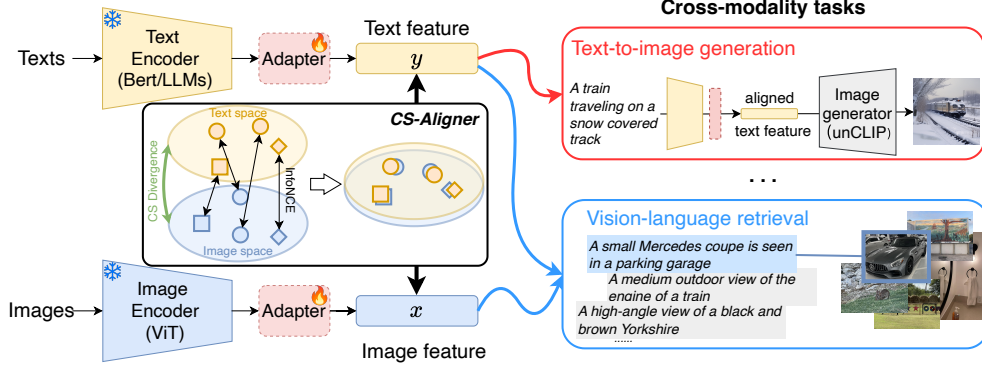


Figure 3: **Illustration of CS-Aligner.** We achieve vision-language alignment by freezing the pretrained text and image encoders and applying parameter-efficient fine-tuning methods (e.g., adapter) with our CS-Aligner. CS-Aligner optimizes the adapters using the aggregated CS divergence and InfoNCE, as formulated in Eq. (6). Once aligned, the adapters are utilized for various cross-modality tasks: the aligned text adapter facilitates text-to-image generation without additional modifications, while the aligned multimodal adapters are used for vision-language retrieval.

Hence, CS-Aligner remains reliable even when the two distributions initially have limited overlap, a common scenario in multimodal tasks. Additionally, its symmetry and non-parametric estimation properties ensure consistent and unbiased multimodal alignment. Consequently, our method ensures both semantic and distributional alignment, enabling robust and efficient multimodal learning.

When estimating the mutual information term  $I(\mathbf{x}, \mathbf{y})$  via InfoNCE (Eq. (2)), unlike other distribution divergences, CS divergence effectively addresses InfoNCE’s inherent alignment–uniformity conflict.

**Uniformity and Alignment with CS Divergence.** Using the Gaussian kernel  $\kappa_t(\mathbf{x}, \mathbf{y}) = \exp(-t\|\mathbf{x} - \mathbf{y}\|_2^2)$  for CS divergence and combining the alignment and uniformity components of InfoNCE, the full objective of Eq. (6) can be expressed as

$$\begin{aligned} \mathcal{L} = & \mathbb{E}_{(\mathbf{x}, \mathbf{y}) \sim p_{\text{pos}}} [\|\mathbf{x} - \mathbf{y}\|_2^\alpha] + \log \mathbb{E}_{\mathbf{x} \sim p(\mathbf{x}), \mathbf{y} \sim p(\mathbf{y})} [\kappa_t(\mathbf{x}, \mathbf{y})] \\ & + \lambda \left( \log \mathbb{E}_{\mathbf{x}, \mathbf{x}' \sim p(\mathbf{x})} [\kappa_t(\mathbf{x}, \mathbf{x}')] + \log \mathbb{E}_{\mathbf{y}, \mathbf{y}' \sim p(\mathbf{y})} [\kappa_t(\mathbf{y}, \mathbf{y}')] - 2 \log \mathbb{E}_{\mathbf{x} \sim p(\mathbf{x}), \mathbf{y} \sim p(\mathbf{y})} [\kappa_t(\mathbf{x}, \mathbf{y})] \right). \end{aligned} \quad (9)$$

When  $\lambda = 1$ , this reduces to the following alignment–uniformity decomposition:

$$\begin{aligned} \mathcal{L} = & \underbrace{\mathbb{E}_{(\mathbf{x}, \mathbf{y}) \sim p_{\text{pair}}} [\|\mathbf{x} - \mathbf{y}\|_2^\alpha] - \log \mathbb{E}_{\mathbf{x} \sim p(\mathbf{x}), \mathbf{y} \sim p(\mathbf{y})} [\exp(-t\|\mathbf{x} - \mathbf{y}\|_2^2)]}_{\text{Alignment}} \\ & + \underbrace{\log \mathbb{E}_{\mathbf{x}, \mathbf{x}' \sim p(\mathbf{x})} [\exp(-t\|\mathbf{x} - \mathbf{x}'\|_2^2)]}_{\text{Uniformity on x}} + \underbrace{\log \mathbb{E}_{\mathbf{y}, \mathbf{y}' \sim p(\mathbf{y})} [\exp(-t\|\mathbf{y} - \mathbf{y}'\|_2^2)]}_{\text{Uniformity on y}}. \end{aligned} \quad (10)$$

**Remark 3.1.** For the alignment part, CS-Aligner promotes both the matching of image-text pairs and the alignment of global distributions. For uniformity, CS-Aligner encourages dispersion within each modality independently, rather than across modalities, which could otherwise conflict with the alignment objective. Thus, our method simultaneously fosters both alignment and uniformity while avoiding the potential conflicts inherent in InfoNCE.

**Remark 3.2.** The connection between CS divergence and InfoNCE becomes evident when analyzing both terms from a cosine similarity perspective. For a characteristic kernel  $\kappa(\mathbf{x}, \mathbf{y}) = \langle \phi(\mathbf{x}), \phi(\mathbf{y}) \rangle_{\mathcal{H}}$ , where  $\phi$  maps samples to a Reproducing Kernel Hilbert Space (RKHS)  $\mathcal{H}$ , the mean embeddings are:  $\boldsymbol{\mu}_x = \frac{1}{m} \sum_{i=1}^m \phi(\mathbf{x}_i)$  and  $\boldsymbol{\mu}_y = \frac{1}{n} \sum_{i=1}^n \phi(\mathbf{y}_i)$ . The CS divergence can then be expressed as:

$$\hat{D}_{\text{CS}}(p(\mathbf{x}); p(\mathbf{y})) = -2 \log \left( \frac{\langle \boldsymbol{\mu}_x, \boldsymbol{\mu}_y \rangle_{\mathcal{H}}}{\|\boldsymbol{\mu}_x\|_{\mathcal{H}} \|\boldsymbol{\mu}_y\|_{\mathcal{H}}} \right) = -2 \log \text{sim}(\boldsymbol{\mu}_x, \boldsymbol{\mu}_y), \quad (11)$$

which evaluates the cosine similarity between distributions in RKHS. Similarly, InfoNCE evaluates cosine similarity between paired samples (Eq. (2)). This dual-level similarity assessment underscores the synergy between CS divergence and mutual information, offering a unified and robust framework for multimodal alignment.

Therefore, CS divergence is compatible with InfoNCE and effectively addresses the inherent conflict between uniformity and alignment, a property not shared by other distribution distance metrics. Detailed comparisons with other metrics are provided in the Appendix D.

### 3.2 Extend CS-Aligner to unpaired data

Benefits from the distributional alignment, we further propose extensions of CS-Aligner, which leverage additional information in unpaired data. While the mutual information estimation (InfoNCE) part requires pairwise data, the CS divergence estimator (Eq. (8)) can operate seamlessly on unpaired data without introducing additional computation. This unique capability enables CS-Aligner to extend beyond traditional pairwise multimodal alignment by incorporating additional distributional information from unpaired data or tokens. Below, we introduce two novel directions.

**Unpaired vision-language alignment.** Our method leverages two forms of unpaired alignments: (1) images with multiple captions, and (2) independently sampled unpaired images and texts. The unpaired alignments are achieved using Eq. (8), where  $\{x_i\}_{i=1}^M$  and  $\{y_j\}_{j=1}^N$  can be independent with  $M \neq N$ . In both scenarios, our method leverages more uncurated unpaired data for distributional multimodal alignment, providing greater flexibility and robustness.

**Vision-language token alignment.** We propose a novel intra-sample distribution alignment approach between vision and language tokens. Unlike CLIP-based models [6] which align only the “CLS” tokens of vision and text representations, the method considers all vision and text tokens for a more fine-grained alignment. Specifically, each vision feature  $\mathbf{x}_i \in \mathbb{R}^{V \times D}$  is modeled as a token distribution  $p(\mathbf{x}_i)$  containing  $V$  vision tokens, while each text feature  $\mathbf{y}_i \in \mathbb{R}^{L \times D}$  is represented as a token distribution  $p(\mathbf{y}_i)$  with  $L$  text tokens.  $D$  denotes the feature dimension. We compute CS divergence between vision and text token distributions, and obtain internal token-wise alignment loss:

$$\mathcal{L}_{\text{token}} = \frac{1}{B} \sum_{i=1}^B \hat{D}_{\text{CS}}(p(\mathbf{x}_i); p(\mathbf{y}_i)), \quad (12)$$

where  $B$  is the batch size. In general,  $V \neq L$ , and vision and language tokens do not have a direct pairing, making InfoNCE inapplicable for estimation. Through our distributional alignment, Eq. (12) enables comprehensive alignment across all tokens, capturing more details and potentially enhancing fine-grained alignment.

### 3.3 Parameter-efficient multimodal alignment

We demonstrate the effectiveness of our CS-Aligner by performing vision-language alignment in a parameter-efficient manner using pretrained vision and language models, such as CLIP and large language models (LLMs) [25]. To adapt these pretrained models, we employ two widely used frameworks: adapter [13] and LoRA [26]. The adapter and LoRA enable efficient alignment of the multimodal large-scale pretrained models, without requiring extensive computational resources. The whole framework is demonstrated in Fig. 3.

**Adapter alignment.** We add a lightweight transformer [27] on top of the pretrained model as an adapter. The adapter projects text embeddings or image embeddings into a shared space.

**LoRA alignment.** We insert trainable low-rank matrices into the pretrained weights of text encoder. It enables fine-grained adjustments to the representations, aligning them with the other modality.

## 4 Experiments

We evaluate our method on two tasks to illustrate its vision-language alignment ability: text-to-image (T2I) generation in Section 4.1 and image-text retrieval in Section 4.2. Additionally, we provide the image-text classification results in the Appendix G.

### 4.1 Text to image generation

**Datasets.** Following a previous T2I approach [15], we train our method on four datasets: **MSCOCO** [16], **CC3M** [28], **CC12M** [29], and **LAION-HighResolution-5M** [30]. MSCOCO contains 80K

images paired with multiple captions. CC3M and CC12M include about 2.5M and 10M image-text pairs, respectively. LAION-HighResolution comprises 175M high-resolution pairs, from which we select 5M for training. We evaluate the aligned model on the MSCOCO 30K validation set.

**Experimental setup.** We build our method based on unCLIP-style approaches (e.g., DALL-E-2 [3], Karlo [31], Kandinsky [4]). These methods typically train a diffusion prior module on large-scale datasets (hundreds of millions data) to map text representations into the image representation space. The diffused text representations are fed into a separate decoder for image generation.

Differently, CS-Aligner trains an adapter to align text representations to image feature space on small-scale datasets, e.g., MSCOCO (0.08M), CC3M (3M), and CC12M (12M), and LAION-HighRes subset (5M). After alignment, we directly process the aligned text features using the pretrained decoder of the large-scale methods (e.g., Karlo and Kandinsky) to generate images, without additional prior modules or multiple diffusion steps. We evaluate generation quality with the FID score [32], which measures how closely generated images match the real image distribution. This metric is particularly well-suited for evaluating modality alignment, as it directly reflects the distribution distance. Additional details can be found in Appendix F.

**Baselines.** Our baselines consists of both large-scale methods Karlo [31], Kandinsky [4] and recent small-scale alignment method Eclipse [15]. Eclipse streamlines the prior module in Karlo and Kandinsky by employing an  $L_2$  loss for T2I. For fairness, we use the same Transformer adapter as Eclipse and only align the “CLS” tokens, highlighting the advantages of our distributional alignment.

**Comparisons.** We compare our method with both the large-scale diffusion-based methods and the small-scale alignment methods. The results are provided in Table 1. By aligning text representations to image representations on the small MSCOCO data, our method achieves superior T2I generation than the large-scale methods, Karlo and Kandinsky, without any diffusion steps. CS-Aligner also outperforms Eclipse by an obvious margin using either Karlo or Kandinsky decoders. The results demonstrate the effective vision-language alignment capability of our method. Moreover, we compare CS-Aligner with Eclipse across different training datasets. As shown in Table 2, our method performs better across diverse training data (CC3M, CC12M, and LAION-HighRes-5M), underscoring the importance of the modality distribution information for robust alignment.

**Qualitative Visualization.** To further test our method, Fig. 4a shows qualitative visualizations of generated images using Karlo decoder. Our aligned text representations result in more realistic images with stronger semantic consistency with the input sentence, highlighting the effectiveness of CS-Aligner in enhancing alignment. More visualizations are provided in Appendix E.1.

**CS-Aligner with different adaptation approaches.** To demonstrate the robustness of our method across different models, we perform alignments for T2I using both adapter and LoRA. Specifically, we apply LoRA with a low-rank dimension of 8 to every transformer layer in the CLIP text encoder. As shown in Table 3, based on either Karlo or Kandinsky, CS-Aligner with LoRA introduces fewer parameters, while still achieving comparable results compared with the adapter-based one, demonstrating the effectiveness and adaptability of CS-Aligner across different models.

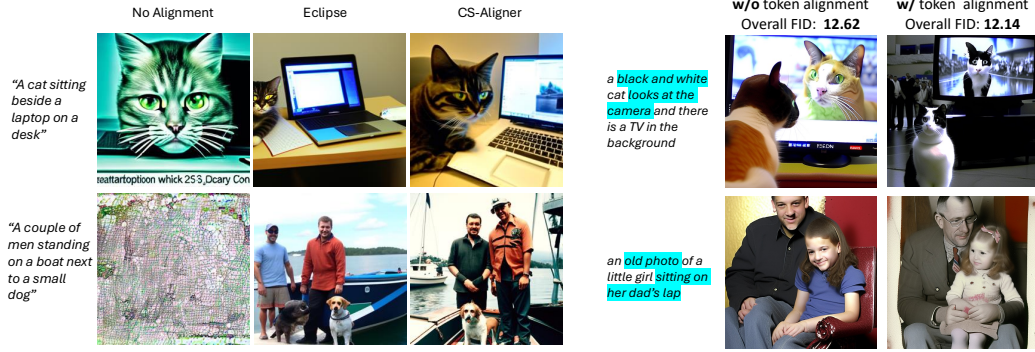
**CS-Aligner with multiple captions.** It is common in real-world datasets for a single image to correspond to multiple captions (e.g., 5 captions per image in MSCOCO). Due to their pairwise alignment nature, previous methods such as InfoNCE and  $\ell_2$ -based approaches [6, 15] struggle to simultaneously leverage multiple captions. In contrast, by incorporating CS divergence, our

Table 1: **Comparisons with T2I methods.** Our method outperforms both large-scale diffusion-based methods (Karlo, Kandinsky) and the recent small-scale method Eclipse.

Methods	Datasize (M)	FID
<b>Large-scale methods</b>		
DALL-E2	250	10.65
Kandinsky	177	20.48
Karlo	115	20.64
<b>Small-scale alignment</b>		
Eclipse + Kandinsky decoder	0.08 <sub>(COCO)</sub>	16.53
Ours + Kandinsky decoder	0.08 <sub>(COCO)</sub>	<b>12.62</b>
Eclipse + Karlo decoder	0.08 <sub>(COCO)</sub>	23.67
Ours + Karlo decoder	0.08 <sub>(COCO)</sub>	<b>11.27</b>

Table 2: **Comparisons on various training data.** Our method consistently performs better.

Method	CC3M	CC12M	LAION-HighRes 5M
Eclipse	26.73	26.98	19.16
Ours	<b>22.88</b>	<b>22.72</b>	<b>14.79</b>



(a) **Qualitative comparison.** No alignment (left), Eclipse (middle), and CS-Aligner (right). CS-Aligner yields more realistic, semantically consistent generations. (b) **CS-Aligner with token alignment.** Token alignment enhances fine-grained vision-language correspondence.

Figure 4: Qualitative visualizations.

CS-Aligner enables training for alignment with single image and multiple captions through the divergence term. To demonstrate the benefits of multiple captions for CS-Aligner, we conducted experiments on the MSCOCO dataset by estimating the CS divergence term  $\hat{D}_{CS}$  in Eq. (6) using both single and multiple captions. As shown in Fig. 5a, CS-Aligner effectively leverages the information provided by multiple captions, leading to improved vision-language alignment.

#### CS-Aligner with additional unpaired data.

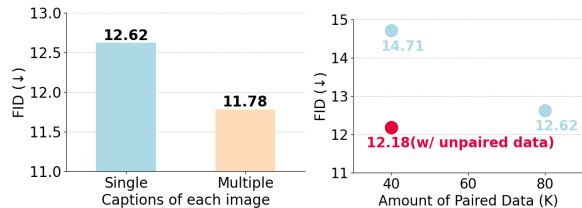
Collecting and accurately annotating paired vision-language data is both challenging and costly. Enhancing alignment with additional unpaired data offers a more flexible and scalable solution for real-world applications. However, similar to the case of multiple captions, previous methods [6, 15] struggle to fully utilize unpaired data due to their reliance on pairwise alignment, whereas CS-Aligner naturally incorporates the unpaired data information by CS divergence. To demonstrate this capability, we conduct experiments on the MSCOCO dataset using the Kandinsky decoder with (1) 80K paired training samples, (2) 40K paired training samples, and (3) 40K paired training samples supplemented with 80K unpaired samples, where the unpaired samples are used to estimate the CS divergence. As shown in Fig. 5b, the result with 40K paired training data is lower than 80K. However, introducing additional unpaired data obviously improves the performance, even surpassing the model trained with 80K paired samples. This demonstrates CS-Aligner’s ability to effectively leverage the distributional information of modalities for alignment.

#### CS-Aligner with token alignment.

Beyond the unpaired data, CS-Aligner also enables token-level alignment by treating the tokens of each sample as a distribution. We evaluated the token-level extension of CS-Aligner using the Kandinsky decoder on the MSCOCO dataset. As shown in Fig. 4b, incorporating token alignment further improves performance. Moreover, qualitative results indicate that token alignment enhances fine-grained details in generated images, suggesting an improved ability to capture fine-grained relationships between modalities. Additional visualizations are provided in Fig. 7 in Appendix E.2.

Table 3: **CS-Aligner with different adaptation approaches.** Our method achieves good alignment using both adapter and LoRA.

Base Model	Adaptation	#Parameters	FID
Kandinsky	Adapter	34M	12.62
	LoRA	6M	13.52
Karlo	Adapter	33M	11.27
	LoRA	1.3M	15.63



(a) Align with multiple captions. (b) Align with unpaired data.

Figure 5: **CS-Aligner with additional information.** Our method benefits from the additional information from multiple captions (a) and unpaired data (b).

## 4.2 Image-Text Retrieval

**Experimental Setup.** Effective multimodal alignment also benefits cross-model retrieval. To demonstrate the alignment ability of our method on retrieval tasks, we align LLMs [25] text representations with CLIP vision representations on both image-to-text and text-to-image retrieval. We use the Flickr 1K test set [33] for short-text retrieval, while Urban1K [34] and DOCCI [35] are employed for long-text retrieval. We compare CS-Aligner against pure InfoNCE-based methods, such as Long-CLIP [34] and LLM2CLIP [1], as the baselines. To ensure a fair comparison, we adopt the setup from LLM2CLIP, aligning CLIP ViT-L/14 image representations with Llama 3 (8B) text representations. Both the vision and text representations are aligned by adapters trained on the CC3M dataset.

**Comparisons.** Table 4 shows that our method consistently and significantly outperforms the baselines across various datasets for both image-to-text (I2T) and text-to-image (T2I) retrieval. This demonstrates the effectiveness of our method for aligning two modalities into a shared space. Moreover, the ability to align a different text encoder (LLM) with the CLIP image encoder highlights the flexibility and generalizability of our approach.

Table 4: **Comparisons of image-to-text (I2T) and text-to-image (T2I) retrieval.** Our method outperforms the baselines on diverse datasets.

Methods	Flickr30k		Urban-1k		DOCCI		Average	
	I2T	T2I	I2T	T2I	I2T	T2I	I2T	T2I
Long-CLIP	90.0	76.2	82.5	86.1	66.5	78.6	79.7	80.3
CLIP	85.2	65.0	68.3	55.6	63.1	65.8	72.2	62.1
LLM2CLIP-3M	89.6	77.3	87.1	91.1	84.9	87.8	87.2	85.4
Ours-3M	<b>91.8</b>	<b>81.0</b>	<b>87.6</b>	<b>92.2</b>	<b>86.6</b>	<b>89.1</b>	<b>88.7</b>	<b>87.4</b>

## 5 Related work

**Vision-language alignment and applications.** CLIP [6] serves as a foundational model for vision-language alignment in multimodal tasks. Several works have enhanced CLIP through techniques such as momentum distillation [36] and noisy text supervision [37]. Despite its success, CLIP suffers from a persistent modality gap between text and image representations. Prior studies [10–12] attribute this gap to factors such as cone effects [11] and suboptimal latent space structures [12]. To address this, various strategies have been proposed, including projection adapters [1, 10, 13], geodesic multimodal mixup [14], and parameter-efficient fine-tuning [38]. Recent works also improve CLIP by large language models (LLMs) [1, 2, 39] for downstream tasks such as **image-text retrieval**.

In addition to image-text retrieval, **text-to-image (T2I) generation** is another application that reflects the vision-language alignment capability. T2I has advanced significantly over the past decades, driven by both diffusion-based [40–43] and GAN-based models [44, 45]. Among diffusion-based methods, the unCLIP framework [3, 40] employs a two-stage architecture with a CLIP-guided diffusion prior and a decoder (e.g., DALL-E-2 [3] or Karlo [31]). Its prior module  $g_\phi$  maps text representations  $\mathbf{y}$  to image ones  $\mathbf{x}$  by a diffusion model. Recently, Eclipse [15] employs an  $\ell_2$  loss to simplify the prior loss by eliminating diffusion time and intruding a noise  $\epsilon$  term:  $\mathcal{L}_{\text{prior}} = \mathbb{E}_{\epsilon \sim \mathcal{N}(0, I)} [\|\mathbf{x} - g_\phi(\epsilon, \mathbf{y})\|_2^2]$ . However, these methods still rely on pairwise loss (e.g.,  $\ell_2$ ). In contrast, our approach introduces distributional alignment for a more holistic modality alignment.

**Cauchy-Schwarz (CS) divergence.** CS divergence [18, 23] is derived from the Cauchy-Schwarz inequality for square-integrable functions. It serves as a symmetric distribution distance metric with notable properties, such as the ability to measure conditional distributions [46] and the closed-form expression for mixtures of Gaussians [47]. CS divergence has been successfully applied across various domains, including deep clustering [48], disentangled representation learning [49], and deep regression [50]. Moreover, due to its advantage of estimating discrepancy between conditional distributions, it has demonstrated success in the domain adaption area [51] and time series clustering [46]. However, the utility of CS divergence in foundation models remains unclear and unexplored.

## 6 Conclusion

In this paper, we propose CS-Aligner, a novel distributional alignment framework that integrates Cauchy-Schwarz (CS) divergence with mutual information for multimodal alignment, which addresses the alignment and uniformity conflict of InfoNCE. By combining global distributional



alignment with InfoNCE, CS-Aligner achieves tighter and more comprehensive alignment. By considering the modality distributional information, our method enables to leverage additional and detailed information from unpaired samples and tokens, leading to more flexible and fine-grained information for alignment. We demonstrate the effectiveness of our alignment on text-to-image generation and cross-modal retrieval.

**Limitation & future work.** Though our method has numerous applications, it is currently evaluated only on unCLIP-type models for generation. In future, we will explore its integration with stable-diffusion-based models. Broader modalities (e.g., audio and video) and diverse tasks (e.g., image-to-text generation) could further strengthen alignment and broaden the applicability of CS-Aligner.

## References

- [1] Weiquan Huang, Aoqi Wu, Yifan Yang, Xufang Luo, Yuqing Yang, Liang Hu, Qi Dai, Xiyang Dai, Dongdong Chen, Chong Luo, et al. Llm2clip: Powerful language model unlock richer visual representation. *arXiv preprint arXiv:2411.04997*, 2024. 1, 2, 9
- [2] Andreas Koukounas, Georgios Mastrapas, Michael Günther, Bo Wang, Scott Martens, Isabelle Mohr, Saba Sturua, Mohammad Kalim Akram, Joan Fontanals Martínez, Saahil Ognawala, et al. Jina clip: Your clip model is also your text retriever. *arXiv preprint arXiv:2405.20204*, 2024. 1, 9
- [3] Aditya Ramesh, Prafulla Dhariwal, Alex Nichol, Casey Chu, and Mark Chen. Hierarchical text-conditional image generation with clip latents. *arXiv preprint arXiv:2204.06125*, 1(2):3, 2022. 1, 2, 7, 9, 20
- [4] Anton Razhigaev, Arseniy Shakhmatov, Anastasia Maltseva, Vladimir Arkhipkin, Igor Pavlov, Ilya Ryabov, Angelina Kuts, Alexander Panchenko, Andrey Kuznetsov, and Denis Dimitrov. Kandinsky: an improved text-to-image synthesis with image prior and latent diffusion. *arXiv preprint arXiv:2310.03502*, 2023. 1, 2, 7
- [5] Deyao Zhu, Jun Chen, Xiaoqian Shen, Xiang Li, and Mohamed Elhoseiny. Minigpt-4: Enhancing vision-language understanding with advanced large language models. *arXiv preprint arXiv:2304.10592*, 2023. 1
- [6] Alec Radford, Jong Wook Kim, Chris Hallacy, Aditya Ramesh, Gabriel Goh, Sandhini Agarwal, Girish Sastry, Amanda Askell, Pamela Mishkin, Jack Clark, et al. Learning transferable visual models from natural language supervision. In *International conference on machine learning*, pages 8748–8763. PMLR, 2021. 1, 2, 6, 7, 8, 9
- [7] Ron Mokady, Amir Hertz, and Amit H Bermano. Clipcap: Clip prefix for image captioning. *arXiv preprint arXiv:2111.09734*, 2021. 1
- [8] Xiaohua Zhai, Basil Mustafa, Alexander Kolesnikov, and Lucas Beyer. Sigmoid loss for language image pre-training. In *Proceedings of the IEEE/CVF international conference on computer vision*, pages 11975–11986, 2023. 1
- [9] Quan Sun, Yuxin Fang, Ledell Wu, Xinlong Wang, and Yue Cao. Eva-clip: Improved training techniques for clip at scale. *arXiv preprint arXiv:2303.15389*, 2023. 1
- [10] Chenliang Zhou, Fangcheng Zhong, and Cengiz Öztireli. Clip-pae: projection-augmentation embedding to extract relevant features for a disentangled, interpretable and controllable text-guided face manipulation. In *ACM SIGGRAPH 2023 Conference Proceedings*, pages 1–9, 2023. 1, 2, 9
- [11] Victor Weixin Liang, Yuhui Zhang, Yongchan Kwon, Serena Yeung, and James Y Zou. Mind the gap: Understanding the modality gap in multi-modal contrastive representation learning. *Advances in Neural Information Processing Systems*, 35:17612–17625, 2022. 1, 3, 9
- [12] Peiyang Shi, Michael C Welle, Mårten Björkman, and Danica Kragic. Towards understanding the modality gap in clip. In *ICLR 2023 Workshop on Multimodal Representation Learning: Perks and Pitfalls*, 2023. 1, 9
- [13] Peng Gao, Shijie Geng, Renrui Zhang, Teli Ma, Rongyao Fang, Yongfeng Zhang, Hongsheng Li, and Yu Qiao. Clip-adapter: Better vision-language models with feature adapters. *International Journal of Computer Vision*, 132(2):581–595, 2024. 2, 6, 9, 20, 21
- [14] Changdae Oh, Junhyuk So, Hoyoon Byun, YongTaek Lim, Minchul Shin, Jong-June Jeon, and Kyungwoo Song. Geodesic multi-modal mixup for robust fine-tuning. *Advances in Neural Information Processing Systems*, 36, 2024. 2, 9
- [15] Maitreya Patel, Changhoon Kim, Sheng Cheng, Chitta Baral, and Yezhou Yang. Eclipse: A resource-efficient text-to-image prior for image generations. In *Proceedings of the IEEE/CVF Conference on Computer Vision and Pattern Recognition*, pages 9069–9078, 2024. 2, 6, 7, 8, 9, 17, 20

- [16] Tsung-Yi Lin, Michael Maire, Serge Belongie, James Hays, Pietro Perona, Deva Ramanan, Piotr Dollár, and C Lawrence Zitnick. Microsoft coco: Common objects in context. In *Computer Vision—ECCV 2014: 13th European Conference, Zurich, Switzerland, September 6–12, 2014, Proceedings, Part V 13*, pages 740–755. Springer, 2014. 2, 6
- [17] Tianhong Li, Sangnie Bhardwaj, Yonglong Tian, Han Zhang, Jarred Barber, Dina Katabi, Guillaume Lajoie, Huiwen Chang, and Dilip Krishnan. Leveraging unpaired data for vision-language generative models via cycle consistency. *arXiv preprint arXiv:2310.03734*, 2023. 2
- [18] Jose C Principe, Dongxin Xu, Qun Zhao, and John W Fisher. Learning from examples with information theoretic criteria. *Journal of VLSI signal processing systems for signal, image and video technology*, 26:61–77, 2000. 2, 4, 9
- [19] Emanuel Parzen. On estimation of a probability density function and mode. *The annals of mathematical statistics*, 33(3):1065–1076, 1962. 2, 4
- [20] Aaron van den Oord, Yazhe Li, and Oriol Vinyals. Representation learning with contrastive predictive coding. *arXiv preprint arXiv:1807.03748*, 2018. 2, 3
- [21] Thomas M Cover. *Elements of information theory*. John Wiley & Sons, 1999. 3
- [22] Tongzhou Wang and Phillip Isola. Understanding contrastive representation learning through alignment and uniformity on the hypersphere. In *International conference on machine learning*, pages 9929–9939. PMLR, 2020. 3, 15
- [23] Jose C Principe, Dongxin Xu, John Fisher, and Simon Haykin. Information theoretic learning. *Unsupervised adaptive filtering*, 1:265–319, 2000. 4, 9
- [24] Robert Jenssen, Jose C Principe, Deniz Erdogmus, and Torbjørn Eltoft. The cauchy–schwarz divergence and parzen windowing: Connections to graph theory and mercer kernels. *Journal of the Franklin Institute*, 343(6):614–629, 2006. 4
- [25] Abhimanyu Dubey, Abhinav Jauhri, Abhinav Pandey, Abhishek Kadian, Ahmad Al-Dahle, Aiesha Letman, Akhil Mathur, Alan Schelten, Amy Yang, Angela Fan, et al. The llama 3 herd of models. *arXiv preprint arXiv:2407.21783*, 2024. 6, 9
- [26] Edward J Hu, Yelong Shen, Phillip Wallis, Zeyuan Allen-Zhu, Yuanzhi Li, Shean Wang, Lu Wang, and Weizhu Chen. Lora: Low-rank adaptation of large language models. *arXiv preprint arXiv:2106.09685*, 2021. 6
- [27] A Vaswani. Attention is all you need. *Advances in Neural Information Processing Systems*, 2017. 6
- [28] Piyush Sharma, Nan Ding, Sebastian Goodman, and Radu Soricut. Conceptual captions: A cleaned, hypernymed, image alt-text dataset for automatic image captioning. In *Proceedings of the 56th Annual Meeting of the Association for Computational Linguistics (Volume 1: Long Papers)*, pages 2556–2565, 2018. 6
- [29] Soravit Changpinyo, Piyush Sharma, Nan Ding, and Radu Soricut. Conceptual 12m: Pushing web-scale image-text pre-training to recognize long-tail visual concepts. In *Proceedings of the IEEE/CVF conference on computer vision and pattern recognition*, pages 3558–3568, 2021. 6
- [30] Christoph Schuhmann, Romain Beaumont, Richard Vencu, Cade Gordon, Ross Wightman, Mehdi Cherti, Theo Coombes, Aarush Katta, Clayton Mullis, Mitchell Wortsman, et al. Laion-5b: An open large-scale dataset for training next generation image-text models. *Advances in Neural Information Processing Systems*, 35:25278–25294, 2022. 6
- [31] Lee Donghoon, Kim Jiseob, Choi Jisu, Kim Jongmin, Byeon Minwoo, Baek Woonhyuk, and Kim Saehoon. Karlo-v1.0.alpha on coyo-100m and cc15m. <https://github.com/kakaobrain/karlo>, 2022. 7, 9
- [32] Martin Heusel, Hubert Ramsauer, Thomas Unterthiner, Bernhard Nessler, and Sepp Hochreiter. Gans trained by a two time-scale update rule converge to a local nash equilibrium. *Advances in neural information processing systems*, 30, 2017. 7

- [33] Peter Young, Alice Lai, Micah Hodosh, and Julia Hockenmaier. From image descriptions to visual denotations: New similarity metrics for semantic inference over event descriptions. *Transactions of the Association for Computational Linguistics*, 2:67–78, 2014. 9
- [34] Beichen Zhang, Pan Zhang, Xiaoyi Dong, Yuhang Zang, and Jiaqi Wang. Long-clip: Unlocking the long-text capability of clip. In *European Conference on Computer Vision*, pages 310–325. Springer, 2025. 9
- [35] Yasumasa Onoe, Sunayana Rane, Zachary Berger, Yonatan Bitton, Jaemin Cho, Roopal Garg, Alexander Ku, Zarana Parekh, Jordi Pont-Tuset, Garrett Tanzer, et al. Docci: Descriptions of connected and contrasting images. In *European Conference on Computer Vision*, pages 291–309. Springer, 2025. 9
- [36] Junnan Li, Ramprasaath Selvaraju, Akhilesh Gotmare, Shafiq Joty, Caiming Xiong, and Steven Chu Hong Hoi. Align before fuse: Vision and language representation learning with momentum distillation. *Advances in neural information processing systems*, 34:9694–9705, 2021. 9
- [37] Chao Jia, Yinfei Yang, Ye Xia, Yi-Ting Chen, Zarana Parekh, Hieu Pham, Quoc Le, Yun-Hsuan Sung, Zhen Li, and Tom Duerig. Scaling up visual and vision-language representation learning with noisy text supervision. In *International conference on machine learning*, pages 4904–4916. PMLR, 2021. 9
- [38] Maxime Zanella and Ismail Ben Ayed. Low-rank few-shot adaptation of vision-language models. In *Proceedings of the IEEE/CVF Conference on Computer Vision and Pattern Recognition*, pages 1593–1603, 2024. 9
- [39] Young Kyun Jang, Junmo Kang, Yong Jae Lee, and Donghyun Kim. Mate: Meet at the embedding—connecting images with long texts. *arXiv preprint arXiv:2407.09541*, 2024. 9
- [40] Aditya Ramesh, Mikhail Pavlov, Gabriel Goh, Scott Gray, Chelsea Voss, Alec Radford, Mark Chen, and Ilya Sutskever. Zero-shot text-to-image generation. In *International conference on machine learning*, pages 8821–8831. Pmlr, 2021. 9
- [41] Robin Rombach, Andreas Blattmann, Dominik Lorenz, Patrick Esser, and Björn Ommer. High-resolution image synthesis with latent diffusion models. In *Proceedings of the IEEE/CVF conference on computer vision and pattern recognition*, pages 10684–10695, 2022.
- [42] Chitwan Saharia, William Chan, Saurabh Saxena, Lala Li, Jay Whang, Emily L Denton, Kamyar Ghasemipour, Raphael Gontijo Lopes, Burcu Karagol Ayan, Tim Salimans, et al. Photorealistic text-to-image diffusion models with deep language understanding. *Advances in neural information processing systems*, 35:36479–36494, 2022.
- [43] Alex Nichol, Prafulla Dhariwal, Aditya Ramesh, Pranav Shyam, Pamela Mishkin, Bob McGrew, Ilya Sutskever, and Mark Chen. Glide: Towards photorealistic image generation and editing with text-guided diffusion models. *arXiv preprint arXiv:2112.10741*, 2021. 9
- [44] Han Zhang, Tao Xu, Hongsheng Li, Shaoting Zhang, Xiaogang Wang, Xiao lei Huang, and Dimitris N Metaxas. Stackgan: Text to photo-realistic image synthesis with stacked generative adversarial networks. In *Proceedings of the IEEE international conference on computer vision*, pages 5907–5915, 2017. 9
- [45] Ming Tao, Bing-Kun Bao, Hao Tang, and Changsheng Xu. Galip: Generative adversarial clips for text-to-image synthesis. In *Proceedings of the IEEE/CVF Conference on Computer Vision and Pattern Recognition*, pages 14214–14223, 2023. 9
- [46] Shujian Yu, Hongming Li, Sigurd Løkse, Robert Jenssen, and José C Príncipe. The conditional cauchy-schwarz divergence with applications to time-series data and sequential decision making. *IEEE Transactions on Pattern Analysis and Machine Intelligence*, 2025. 9
- [47] Kittipat Kampa, Erion Hasanbelliu, and Jose C Principe. Closed-form cauchy-schwarz pdf divergence for mixture of gaussians. In *The 2011 International Joint Conference on Neural Networks*, pages 2578–2585. IEEE, 2011. 9

- [48] Daniel J Trosten, Sigurd Lokse, Robert Jenssen, and Michael Kampffmeyer. Reconsidering representation alignment for multi-view clustering. In *Proceedings of the IEEE/CVF conference on computer vision and pattern recognition*, pages 1255–1265, 2021. 9
- [49] Linh Tran, Maja Pantic, and Marc Peter Deisenroth. Cauchy-schwarz regularized autoencoder. *Journal of Machine Learning Research*, 23, 2022. 9
- [50] Shujian Yu, Xi Yu, Sigurd Løkse, Robert Jenssen, and Jose C Principe. Cauchy-schwarz divergence information bottleneck for regression. *arXiv preprint arXiv:2404.17951*, 2024. 9
- [51] Wenzhe Yin, Shujian Yu, Yicong Lin, Jie Liu, Jan-Jakob Sonke, and Stratis Gavves. Domain adaptation with cauchy-schwarz divergence. In *The 40th Conference on Uncertainty in Artificial Intelligence*, 2024. 9, 18
- [52] Qing Wang, Sanjeev R Kulkarni, and Sergio Verdú. Divergence estimation for multidimensional densities via  $k$ -nearest-neighbor distances. *IEEE Transactions on Information Theory*, 55(5):2392–2405, 2009. 17
- [53] Martin Arjovsky, Soumith Chintala, and Léon Bottou. Wasserstein generative adversarial networks. In *International conference on machine learning*, pages 214–223. PMLR, 2017. 18
- [54] Alexander Korotin, Daniil Selikhanovych, and Evgeny Burnaev. Neural optimal transport. *arXiv preprint arXiv:2201.12220*, 2022. 18
- [55] Marco Cuturi. Sinkhorn distances: Lightspeed computation of optimal transport. *Advances in neural information processing systems*, 26, 2013. 18
- [56] Jin-Hwa Kim, Yunji Kim, Jiyoung Lee, Kang Min Yoo, and Sang-Woo Lee. Mutual information divergence: A unified metric for multimodal generative models. *Advances in Neural Information Processing Systems*, 35:35072–35086, 2022. 18
- [57] Chuanxia Zheng, Tung-Long Vuong, Jianfei Cai, and Dinh Phung. Movq: Modulating quantized vectors for high-fidelity image generation. *Advances in Neural Information Processing Systems*, 35:23412–23425, 2022. 18
- [58] Jonathan Ho, Ajay Jain, and Pieter Abbeel. Denoising diffusion probabilistic models. *Advances in neural information processing systems*, 33:6840–6851, 2020. 18
- [59] Jonathan Ho and Tim Salimans. Classifier-free diffusion guidance. *arXiv preprint arXiv:2207.12598*, 2022. 18



## A Broader Impacts

Our proposed method advances research in multimodal alignment by introducing a novel distributional alignment approach. As a result, it also facilitates progress in multimodal generation. In the meantime, this capability may raise ethical concerns, including the potential misuse for generating deceptive or inappropriate content.

## B Details of the toy examples

**Example B.1.** Consider two Gaussian distributions,  $p(\mathbf{x}) \sim \mathcal{N}(\mu_{\mathbf{x}}, \sigma_{\mathbf{x}}^2)$  and  $p(\mathbf{y}) \sim \mathcal{N}(\mu_{\mathbf{y}}, \sigma_{\mathbf{y}}^2)$ , with a joint distribution  $p(\mathbf{x}, \mathbf{y}) \sim \mathcal{N}\left(\begin{pmatrix} \mu_{\mathbf{x}} \\ \mu_{\mathbf{y}} \end{pmatrix}, \begin{pmatrix} \sigma_{\mathbf{x}}^2 & \rho\sigma_{\mathbf{x}}\sigma_{\mathbf{y}} \\ \rho\sigma_{\mathbf{x}}\sigma_{\mathbf{y}} & \sigma_{\mathbf{y}}^2 \end{pmatrix}\right)$ . Here,  $\mu_{\mathbf{x}}$  and  $\mu_{\mathbf{y}}$  are the means of  $\mathbf{x}$  and  $\mathbf{y}$ ,  $\sigma_{\mathbf{x}}^2$  and  $\sigma_{\mathbf{y}}^2$  are their variances, and  $\rho$  is the correlation coefficient and controls their linear dependency. When  $\rho = 0.99$ , the two modalities are highly dependent, with high mutual information ( $I = 1.959$ ; see Fig. 2a and 2b). When  $\rho = 0$ , the modalities are independent, resulting in zero mutual information (Fig. 2c). Interestingly, two distributions with the same mutual information value can either exhibit minimal statistical distance and nearly identical shapes, including similar locations, widths, and higher-order moments, as shown in Fig. 2b, or have completely different shapes with distinct means (0 for  $p(\mathbf{x})$  and 2 for  $p(\mathbf{y})$ ) and variances (4 for  $p(\mathbf{x})$  and 1 for  $p(\mathbf{y})$ ), as illustrated in Fig. 2a. Quantitatively, the former case shows a minimal KL divergence of 0, while the latter exhibits a KL divergence of nearly 6.81.

**Mutual information.** For two continuous random variables  $\mathbf{x}$  and  $\mathbf{y}$ , the mutual information is defined as:

$$I(\mathbf{x}; \mathbf{y}) = \iint p(\mathbf{x}, \mathbf{y}) \log\left(\frac{p(\mathbf{x}, \mathbf{y})}{p(\mathbf{x})p(\mathbf{y})}\right) d\mathbf{x} d\mathbf{y}. \quad (13)$$

For a bivariate Gaussian distribution

$$p(\mathbf{x}, \mathbf{y}) \sim \mathcal{N}\left(\begin{pmatrix} \mu_{\mathbf{x}} \\ \mu_{\mathbf{y}} \end{pmatrix}, \begin{pmatrix} \sigma_{\mathbf{x}}^2 & \rho\sigma_{\mathbf{x}}\sigma_{\mathbf{y}} \\ \rho\sigma_{\mathbf{x}}\sigma_{\mathbf{y}} & \sigma_{\mathbf{y}}^2 \end{pmatrix}\right),$$

the mutual information admits the closed-form solution:

$$I(\mathbf{x}; \mathbf{y}) = -\frac{1}{2} \ln(1 - \rho^2). \quad (14)$$

In particular, for correlation  $\rho = 0.99$ , we have  $I(\mathbf{x}, \mathbf{y}) \approx 1.959$ , while for  $\rho = 0$ , the variables are independent and  $I(\mathbf{x}, \mathbf{y}) = 0$ .

**Divergence.** For univariate Gaussian distributions  $p(\mathbf{x}) = \mathcal{N}(\mu_{\mathbf{x}}, \sigma_{\mathbf{x}}^2)$  and  $p(\mathbf{y}) = \mathcal{N}(\mu_{\mathbf{y}}, \sigma_{\mathbf{y}}^2)$ , the KL divergence is given by:

$$D_{\text{KL}}(p(\mathbf{x}) \| p(\mathbf{y})) = \ln\left(\frac{\sigma_{\mathbf{y}}}{\sigma_{\mathbf{x}}}\right) + \frac{\sigma_{\mathbf{x}}^2 + (\mu_{\mathbf{x}} - \mu_{\mathbf{y}})^2}{2\sigma_{\mathbf{y}}^2} - \frac{1}{2}. \quad (15)$$

For Fig. 2b and Fig. 2c, we set  $\sigma_{\mathbf{x}} = \sigma_{\mathbf{y}} = 1$ . Hence, when  $\mu_{\mathbf{x}} = \mu_{\mathbf{y}} = 0$ ,  $D_{\text{KL}}(p(\mathbf{x}) \| p(\mathbf{y})) = 0$ .

For Fig. 2a, we use  $\sigma_{\mathbf{x}} = 2$  and  $\sigma_{\mathbf{y}} = 1$ . When  $\mu_{\mathbf{x}} = 0$  and  $\mu_{\mathbf{y}} = 2$ , the  $D_{\text{KL}}(p(\mathbf{x}) \| p(\mathbf{y})) \approx 6.81$ , which is very large.

## C Derivations

In this section, we provide a derivation of alignment and uniformity terms of InfoNCE. More concrete analysis can be found in [22].

Let  $(\mathbf{x}, \mathbf{y})$  be positive (image–text) pairs drawn from  $p_{\text{pair}}$ , and let  $\{(\mathbf{x}'_i, \mathbf{y}'_i)\}_{i=1}^M$  be  $M$  negative samples (unpaired samples) drawn i.i.d. from the marginal  $p_{\text{data}}$ . The one-sided InfoNCE (CLIP) loss with temperature  $\tau > 0$  is

$$\mathcal{L}_{\text{InfoNCE}} = -\frac{1}{2} \mathbb{E}_{(\mathbf{x}, \mathbf{y}) \sim p_{\text{pair}}} \mathbb{E}_{\{(\mathbf{x}'_i, \mathbf{y}'_i)\}_{i=1}^M \sim p_{\text{data}}} \left[ \log \frac{e^{\mathbf{x}^\top \mathbf{y} / \tau}}{\sum_{i=1}^M e^{\mathbf{x}'_i^\top \mathbf{y} / \tau}} + \log \frac{e^{\mathbf{x}^\top \mathbf{y} / \tau}}{\sum_{i=1}^M e^{\mathbf{x}^\top \mathbf{y}'_i / \tau}} \right].$$

In CLIP, the features are normalized to compute the loss. Under this unit-norm constraint  $\|\mathbf{x}\|_2 = \|\mathbf{y}\|_2 = 1$ ,  $\mathcal{L}_{\text{InfoNCE}}$  decomposes into

$$\mathcal{L}_{\text{InfoNCE}} = \underbrace{-\mathbb{E}_{(\mathbf{x}, \mathbf{y}) \sim p_{\text{pair}}} \left[ \frac{\mathbf{x}^\top \mathbf{y}}{\tau} \right]}_{\mathcal{L}_{\text{align}}} + \underbrace{\mathbb{E}_{(\mathbf{x}, \mathbf{y}) \sim p_{\text{data}}} \left[ \frac{1}{2} \log \sum_{i=1}^M e^{\mathbf{x}^\top \mathbf{y}'_i / \tau} + \frac{1}{2} \log \sum_{i=1}^M e^{\mathbf{x}'_i{}^\top \mathbf{y} / \tau} \right]}_{\mathcal{L}_{\text{uniform}}},$$

up to an additive constant. Moreover, by writing

$$\|\mathbf{x} - \mathbf{y}\|_2^2 = \|\mathbf{x}\|^2 + \|\mathbf{y}\|^2 - 2\mathbf{x}^\top \mathbf{y} = 2 - 2\mathbf{x}^\top \mathbf{y} \implies \mathbf{x}^\top \mathbf{y} = 1 - \frac{1}{2}\|\mathbf{x} - \mathbf{y}\|_2^2, \quad (16)$$

we can show that:

(i) *Alignment.*

$$-\mathbb{E}_{(\mathbf{x}, \mathbf{y})} \left[ \frac{\mathbf{x}^\top \mathbf{y}}{\tau} \right] = -\mathbb{E} \left[ \frac{1 - \frac{1}{2}\|\mathbf{x} - \mathbf{y}\|_2^2}{\tau} \right] = -\frac{1}{\tau} + \frac{1}{2\tau} \mathbb{E}[\|\mathbf{x} - \mathbf{y}\|_2^2].$$

Dropping the constant  $-1/\tau$ , define

$$\mathcal{L}_{\text{align}} := \frac{1}{2\tau} \mathbb{E}_{(\mathbf{x}, \mathbf{y}) \sim p_{\text{pair}}} [\|\mathbf{x} - \mathbf{y}\|_2^2]. \quad (17)$$

(ii) *Uniformity.* For each negative (unpaired) sample  $\mathbf{y}'_i$ , using Eq. (16),

$$e^{\mathbf{x}^\top \mathbf{y}'_i / \tau} = e^{(1 - \frac{1}{2}\|\mathbf{x} - \mathbf{y}'_i\|_2^2) / \tau} = e^{1/\tau} e^{-\frac{1}{2\tau}\|\mathbf{x} - \mathbf{y}'_i\|_2^2}.$$

Hence

$$\sum_{i=1}^M e^{\mathbf{x}^\top \mathbf{y}'_i / \tau} = e^{1/\tau} \sum_{i=1}^M e^{-\frac{1}{2\tau}\|\mathbf{x} - \mathbf{y}'_i\|_2^2}, \quad \log \sum_{i=1}^M e^{\mathbf{x}^\top \mathbf{y}'_i / \tau} = \frac{1}{\tau} + \log \sum_{i=1}^M e^{-\frac{1}{2\tau}\|\mathbf{x} - \mathbf{y}'_i\|_2^2}.$$

An identical argument holds for the  $\{\mathbf{x}'_i, \mathbf{y}\}$  terms. Up to constants,

$$\mathcal{L}_{\text{uniform}} := \mathbb{E}_{(\mathbf{x}, \mathbf{y}) \sim p_{\text{data}}} \left[ \frac{1}{2} \log \sum_{i=1}^M e^{-\frac{1}{2\tau}\|\mathbf{x} - \mathbf{y}'_i\|_2^2} + \frac{1}{2} \log \sum_{i=1}^M e^{-\frac{1}{2\tau}\|\mathbf{x}'_i - \mathbf{y}\|_2^2} \right]. \quad (18)$$

In the limit of large batch size one may further rewrite

$$\mathcal{L}_{\text{uniform}} \approx \log \mathbb{E}_{\mathbf{x}, \mathbf{y} \sim p_{\text{data}}} [\exp(-t\|\mathbf{x} - \mathbf{y}\|_2^2)],$$

with  $t = \frac{1}{2\tau}$ .

Combining (i) and (ii) and absorbing all additive constants gives the desired decomposition

$$\boxed{\mathcal{L}_{\text{clip}} = \mathcal{L}_{\text{align}} + \mathcal{L}_{\text{uniform}} + \text{const.}}$$

## D Comparison between CS divergence and other metrics

Unlike parametric distributions, distributions of different real-world modalities exhibit unpredictable variability and inconsistent overlaps, meaning that  $p(\mathbf{x})$  and  $p(\mathbf{y})$  may follow arbitrary distributions with a small intersection. Therefore, it is crucial to overcome these challenges to measure and optimize multimodal distribution divergence robustly. Below, we outline several key properties that an effective metric should satisfy for multimodal alignment.

**Remark D.1.** Key properties for distribution align metrics:

- *Symmetry:* Both distributions are treated equally, ensuring consistent and unbiased multimodal alignment, formulated by  $D(p(\mathbf{x}), p(\mathbf{y})) = D(p(\mathbf{y}), p(\mathbf{x}))$ .
- *Differentiable and Efficient Estimation:* Enable differentiable estimation without distribution assumptions to facilitate optimization, formulated as  $\partial D(p(\mathbf{x}; \theta), p(\mathbf{y}; \phi)) \neq \emptyset, \forall p(\mathbf{x}), p(\mathbf{y})$ . Achieve the estimation non-parametrically or efficiently.
- *Robustness to Small Distribution Overlap:* Provide reliable measurements even when distributions have minimal overlap of supports, which may often occur in multimodal scenarios. The property is formulated as  $0 \leq D(p(\mathbf{x}), p(\mathbf{y})) \leq \infty$  when  $0 < \mu(\text{supp}(p(\mathbf{x})) \cap \text{supp}(p(\mathbf{y}))) < \epsilon$ .  $\mu(\text{supp}(p(\mathbf{x})) \cap \text{supp}(p(\mathbf{y})))$  denotes the overlap of  $p(\mathbf{x})$  and  $p(\mathbf{y})$ .  $\epsilon$  is a small value.

These properties enable the divergence term to align arbitrary distributions with small support overlap, which is well-suited for large-scale multimodal applications involving deep learning.

## D.1 Connection to the prior loss

**Remark D.2.** Connection to the prior loss ( $\ell_2$  loss) used by Eclipse [15]:

$$\mathcal{L}_{\text{prior}} = \mathbb{E}_{\epsilon \sim \mathcal{N}(0, I)} \left[ \|\mathbf{x} - g_\phi(\epsilon, \mathbf{y})\|_2^2 \right]. \quad (19)$$

Consider the third term in Eq. (8), which involves  $\kappa(\mathbf{x}_i, \mathbf{y}_j)$  defined by the Gaussian kernel  $\kappa_\sigma(\mathbf{x}, \mathbf{y}) = \exp(-\|\mathbf{x} - \mathbf{y}\|_2^2 / 2\sigma^2)$ . A second-order Taylor expansion yields

$$\kappa(\mathbf{x}_i, \mathbf{y}_j) = \exp\left(-\frac{(\mathbf{x}_i - \mathbf{y}_j)^2}{2\sigma^2}\right) \approx 1 - \frac{(\mathbf{x}_i - \mathbf{y}_j)^2}{2\sigma^2}. \quad (20)$$

When  $i = j$  (i.e., diagonal of  $\kappa(\mathbf{x}, \mathbf{y})$ ), this approximation reduces to a weighted  $\ell_2$  loss by  $1/2\sigma^2$ , analogous to the Eq. 19. Consequently, the  $\ell_2$  loss emerges as a special case of our divergence, focusing solely on paired sample reconstruction and omitting broader distribution alignment, including off-diagonal (cross-sample) contributions.

## D.2 Comparison with KL divergence.

KL divergence is a widely used metric in deep learning. Given two distributions,  $p(\omega)$  and  $q(\omega)$ , the KL divergence is defined as:

$$D_{\text{KL}}(p; q) = \int p(\omega) \log \frac{p(\omega)}{q(\omega)} d\omega \quad (21)$$

**Validity for multimodal alignment.** Define the support sets of distributions  $p$  and  $q$  as:

$$\text{supp}(p) = \{\omega \in \Omega : p(\omega) > 0\}, \quad \text{supp}(q) = \{\omega \in \Omega : q(\omega) > 0\}. \quad (22)$$

For KL divergence, if there exists any point  $x \in \text{supp}(p)$  such that  $q(x) = 0$ , the term  $p(\omega) \log \frac{p(\omega)}{q(\omega)} \rightarrow \infty$ , leading to:  $D_{\text{KL}}(p; q) = \infty$ . Thus, a necessary condition for KL divergence to be finite is  $\text{supp}(p) \subseteq \text{supp}(q)$ . Otherwise, KL divergence becomes invalid.

In contrast, the CS divergence becomes infinite only if there is no overlap between supports of  $p$  and  $q$ , i.e., when  $\int p(\omega)q(\omega)d\omega = 0$ , making the logarithm undefined. Hence, the condition for finite CS divergence is:  $\text{supp}(p) \cap \text{supp}(q) \neq \emptyset$ .

In multimodal alignment, it's reasonable to assume that the two modality distributions partially overlap but are not disjoint, as supported by our empirical observations in Fig. 4a (no alignment results). Under these conditions, KL divergence can be invalid and therefore suboptimal. Conversely, the CS divergence condition is less restrictive, making it more suitable and stable for multimodal alignment.

**Compatibility with InfoNCE** Integrating InfoNCE with CS divergence explicitly encourages intra-modality uniformity and cross-modality alignment, thereby effectively improving multimodal alignment. For KL divergence, assuming the distributions of the two modalities are Gaussian,  $\mathcal{N}(\mu_0, \Sigma_0)$  and  $\mathcal{N}(\mu_1, \Sigma_1)$ , the divergence can be computed as:

$$\mathcal{D}_{\text{KL}}[\mathcal{N}(\mu_0, \Sigma_0) \parallel \mathcal{N}(\mu_1, \Sigma_1)] = \frac{1}{2} \left( \text{tr}(\Sigma_1^{-1}\Sigma_0) + (\mu_1 - \mu_0)^\top \Sigma_1^{-1}(\mu_1 - \mu_0) - k + \log \left( \frac{\det \Sigma_1}{\det \Sigma_0} \right) \right). \quad (23)$$

This formulation lacks explicit connections to the InfoNCE in terms of alignment and uniformity, making it less compatible with InfoNCE compared to the CS divergence.

**Nonparametric estimation.** Additionally, when the distributions are not assumed to be Gaussian, a nonparametric estimator is required for KL divergence. A common choice, the k-NN estimator [52], is non-differentiable, which poses challenges for optimization in gradient-based learning frameworks. In contrast, the CS divergence demonstrates greater stability and differentiability when paired with KDE, making it a more robust choice.

**Experimental Comparison.** To verify the above analysis, we compare CS divergence and KL divergence on the unpaired data scenario, where KL can easily become invalid. We trained a KL

+ InfoNCE model in our unpaired data setting—using paired data for InfoNCE and unpaired data for divergence. The initial KL value exceeded 5000 (extremely large), and consequently, the model could not converge, leading to catastrophic failure. In contrast, CS divergence remained stable (initial value around 3), and achieved comparable final performance with an FID of 12.18 (Fig. 5b in the main paper).

For the scenario

### D.3 Comparison with Wasserstein distance.

Wasserstein Distance is also widely used for distribution discrepancy (e.g. GAN [53]). However, Wasserstein distance is computed either by using an additional learnable module (e.g., a neural network for estimating a transport map [54]) or by solving an optimization problem, often approximated via multiple Sinkhorn [55] iterations for computational efficiency, leading to efficiency problem in large-scale training. In contrast, CS divergence can be efficiently estimated by a nonparametric estimator.

### D.4 Comparison with mutual information divergence [56].

Mutual information estimation depends on parametric assumptions about the underlying distributions—e.g., multivariate Gaussian—whereas CS divergence imposes no such constraints. Moreover, estimating mutual information decomposes into a mutual information term plus two KL divergences, and thus lacks explicit connections to the InfoNCE in terms of alignment and uniformity.

## E More Results

### E.1 More Visualization

We illustrate more high-resolution images generated by the Kandinsky decoder with our aligned text representation in Fig. 6. The adapter is trained on LAION-HighRes 5M.

### E.2 More visualization for token alignment

We provide more visualizations with and without the token alignment Fig. 7, demonstrating its ability to generate more fine-grained images with CS-Aligner.

## F Implementation details

**Implementation details** Our models were trained on 4 NVIDIA RTX A100 GPUs with a global batch size of 1,024 (256 per GPU). We optimized parameters using AdamW with a cosine annealing learning rate schedule, spanning a total of 100 GPU hours. Mixed-precision training (FP16) was employed to enhance computational efficiency while maintaining stability. We use the learning rate of  $5e - 5$ . We use hyperparameter  $\lambda$  as 0.01 to keep the same number scale as the divergence.

**Kernel density estimator.** A proper kernel size is critical in KDE for accurate estimation of Eq. (8). In this paper, we follow [51] to normalize the features from two modalities and use a kernel size 1. In general, this is sufficient to ensure stable learning.

### F.1 T2I details

**Kandinsky details.** We use Kandinsky v2.2, an unCLIP-type model that utilizes CLIP ViT-bigG-14-laion2B-39B-b160k with 1280 projection dimensions for text and image encoders. Kandinsky v2.2 employs a latent diffusion model and MOVQ [57] as the decoder to generate images of size  $512 \times 512$  from the given image representation. When using the Kandinsky decoder, we apply 50 denoising steps [58] with a classifier-free guidance scale of 7.5 [59].

**Karlo details.** Karlo uses CLIP-ViT-L/14 with 768 projection dimensions for image and text encoders. It employs a diffusion model to decode the image representation into a low-resolution

*A vase of flowers displayed at the front windows of a store*



*A bald man with a beard wearing a polka dot bow tie*



*A basket fill with different types of fruit*



*A bedroom decorated with a blue underwater theme*



*A wooden cutting board filled with chopped vegetables*



*"Head shot" of a zebra against a stark background*



*A backpack and a line of supplies laying out*



*A bathroom is very colorful with blue yellow and red*



*A bear made out of gummy bears sitting on a counter*



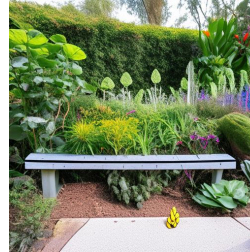
*A bed in a bedroom next to a slide glass door*



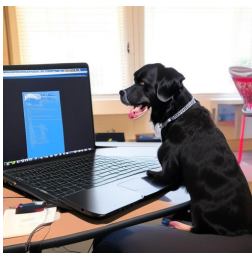
*A bed with a colorful blanket has an iron bed frame*



*a bench surrounded by different types of plant life*



*A big black dog sitting next to a laptop computer*



*A big brown horse near a fence in the snow*



*a big sail boat in the sea with other boats*



*a black and white cat hugging a handbag*



Figure 6: **Qualitative visualization.** The adapter is trained on LAION-HighRes 5M. The aligned text representation is then decoded by the Kandinsky decoder.





Figure 7: **Token alignment is effective for fine-grained generations with more details and stronger semantic correspondence with the text inputs.**

image, followed by a super-resolution diffusion module that upsamples it to  $512 \times 512$ . When using the Karlo decoder, we apply 25 denoising steps with a classifier-free guidance scale of 7.5, followed by an additional 7 super-resolution steps.

**Adapter details.** To ensure a fair comparison, our adapter module has the same architecture as Eclipse [15], which is based on the standard PriorTransformer model [3] but modified to be time-independent. Specifically, it consists of 10 layers with 16 attention heads, each having a head dimension of 32. The embedding dimension is 768/1280, with three additional embeddings. The model does not use time embeddings and has a dropout rate of 0.0. For the text to image generation task, in order to use the pretrained image generator, we only use the text adapter. For the retrieval and classification, we use adapters for both modalities.

**LoRA** We configure LoRA (Low-Rank Adaptation) for CLIP with a rank of  $r = 8$  and a scaling factor of  $\alpha = 16$ , enabling efficient adaptation while maintaining a low computational footprint. The targeted modules include the self-attention projections, the fully connected layers, and the `text_projection` layer, ensuring adaptation across both vision and text processing components. A dropout rate of 0.1 is applied to enhance regularization. For the CLIP encoder in Kandinsky, ViT-bigG-14-laion2B-39B-b160k, the number of LoRA parameters is 6 million. As for CLIP-ViT-L/14 in Karlo, the CLIP model size is smaller, resulting in 1.3 million LoRA parameters.

**LAION-HighResolution-5M selection.** We use a subset of 5 million image-text pairs from the LAION-HighResolution dataset, which contains 175 million pairs. Due to computational constraints, we download only a portion of the dataset and select pairs with English captions.

## G More experimental results

**Image-text classification.** We compare with CLIP-Adapter [13] on the image classification task following their few-shot classification setting. We fine-tune the adapter based on ViT-B/16 with 16-shots subset for each of the 11 datasets. The results are provided in the following table. With better alignment, our method consistently performs better.

**Hyperparameter Sensitivity Analysis.** We conducted a sensitivity analysis on the two key hyperparameters,  $\lambda$  (the weight for InfoNCE) and  $\sigma$  (the Gaussian kernel width). For efficiency, we evaluated on a subset of 10 000 MSCOCO training samples and report Fréchet Inception Distance (FID) as the metric.

Table 5: **Comparison with CLIP-Adapter on the image classification task.** Our methods performs consistently better on various datasets.

Method	ImageNet	Caltech101	DTD	EuroSAT	FGVCAircraft	Food101	Flowers102	OxfordPets	StanfordCars	SUN397	UCF101	Average
[13]	71.1	94.4	70.9	85.7	42.8	83.2	96.0	92.1	78.6	75.0	82.8	79.3
Ours	<b>72.9</b>	<b>95.0</b>	<b>72.3</b>	<b>87.2</b>	<b>44.4</b>	<b>85.8</b>	<b>97.5</b>	<b>93.0</b>	<b>81.9</b>	<b>76.2</b>	<b>84.0</b>	<b>80.9</b>

Table 6 shows that our method is robust to moderate variations in both  $\lambda$  and  $\sigma$ , with only minor FID fluctuations over a wide range.

Table 6: **Sensitivity of FID to  $\lambda$  and  $\sigma$ .**

$\lambda$	0.01	0.1	1	10	$\sigma$	0.1	0.5	1	1.5
FID	81.34	32.51	29.86	65.79	FID	30.58	27.79	29.86	31.49

(a)  $\lambda$  sensitivity
(b)  $\sigma$  sensitivity

**Alignment with InfoNCE is not enough for the generation task.** We train the adapter solely with InfoNCE and use the Kandinsky decoder to generate the corresponding images. Table 7 shows that InfoNCE alone struggles to align the multimodal distributions, resulting in a high FID score.

Table 7: **Ablation study of CS-Aligner.** Alignment with CS-Aligner significantly outperforms the alignment results with only InfoNCE.

Loss	FID
InfoNCE	151.35
CS-Aligner	12.62